

Statistical description of multipion production in diffractive hadronic reactions

R. Gagnon

Physics Department, McGill University, Montréal, Québec H3A 2T8, Canada
and Département de Physique-Mathématiques, Université de Moncton, Centre Universitaire de Moncton, Moncton,
*Nouveau-Brunswick E1A 3E9, Canada**

(Received 6 December 1979)

A statistical model in which higher-multiplicity enhancements are generated from lower ones in a completely determined fashion is presented. Full account is taken of isospin and G -parity conservation as well as the finite width of the produced resonances. It is applied to diffractive dissociation on nucleon and deuteron targets, for which multipion mass distributions and relative cross sections are calculated. Agreement with available experimental data is seen to be excellent.

I. INTRODUCTION

New data on diffractive five-pion production have been published¹ and constitute a good test for statistical models which, at relatively high multiplicity, should provide a good description of the mass distribution of multipion systems. In this paper, we present a generalization of a statistical model proposed by Margolis and collaborators² a few years ago. Specifically, a fireball consisting of an incoherent superposition of overlapping resonances is dynamically formed through Regge exchange in the t channel and then decays statistically and sequentially in the s channel according to the statistical bootstrap model of Hagedorn³ and Frautschi.⁴

The cross section for this process (shown in Fig. 1) is as follows^{5,6}:

$$\frac{d\sigma}{dM^2} = \frac{1}{16\pi\lambda(s, m_a^2, m_b^2)} \frac{1}{M} \times \int dt R(s, t, M) P(F \rightarrow n\pi), \quad (1)$$

where

$$\lambda(x, y, z) = x^2 + y^2 + z^2 - 2xy - 2xz - 2yz, \quad (2)$$

$R(s, t, M)$ is the fireball production matrix element, and $P(F \rightarrow n\pi)$ is the decay probability into n pions. In this picture, a fireball decays according to the relative proportions of its constituents. Since it consists mainly of a heavy particle and one or two light resonances,⁴ we are led to a cascade-decay-type model as depicted in Fig. 1(b). At each step i of the cascade, we associate a decay probability into n bodies:

$$P(M_i) = \frac{\rho_n(M_i)}{\rho(M_i)}, \quad (3)$$

where $\rho_n(M_i)$ is the contribution of the n -particle states to the total density of states $\rho(M_i)$. $P(F \rightarrow n\pi)$ will then be a convolution of all $P(M_i)$'s over the different steps of the cascade. In phase-space language, the total density of states is given by⁴

$$\rho_{\text{out}}(M) = \sum_{n=2}^{\infty} \left[\frac{V}{(2\pi)^3} \right]^{n-1} \frac{1}{n!} \prod_{i=1}^n \int dm_i \rho_{1n}(m_i) \int d^3q_i \delta \left(\sum_{j=1}^n E_j - M \right) \delta^3 \left(\sum_{k=1}^n q_k \right). \quad (4)$$

This equation has been solved in the asymptotic limit using the strong bootstrap condition $\rho_{1n}(M) \xrightarrow{M \rightarrow \infty} \rho_{\text{out}}(M)$ and the result is^{4,7} $\rho(M) = ae^{M/T}/M^3$.

Margolis and Rudaz⁸ and Harris *et al.*¹ applied this model to the three- and five-pion enhancements assuming pion emission only along the decay chain and a pion plus a resonance at the end. While the three-pion spectrum is well described, the five-pion spectrum is less well described and the three-to-five-pion ratio is off by roughly a factor of 2.5. This suggests that many more contributions must be taken into account, for instance,

resonance emission along or at the end of the chain. We thus generalized Eq. (4) to incorporate G -parity and isospin conservation as well as the finite width of the emitted discrete resonances. Using the formalism presented in Sec. II, we developed recursion relations enabling us to calculate explicitly the isospin- and G -parity-dependent total density of states. Applications to diffractive pion-proton scattering at high energy in both the linear (two-particle vertices only) and the nonlinear (two- and three-particle vertices) versions of the model can be found in Sec. III. Up to nine-pion mass spectra were calculated as well as the

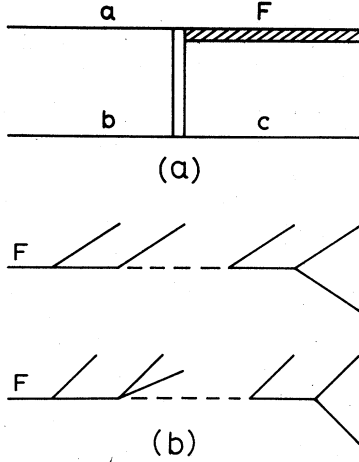


FIG. 1. (a) A fireball is formed through Regge exchange in the t channel. (b) Statistical decay of a fireball in the linear (upper diagram) and in the nonlinear (lower diagram) version of the model.

relative production cross sections. In Sec. IV, similar calculations are performed for a deuterium target at $P_{1ab} = 15$ GeV/c.

II. GENERAL FORMALISM AND CALCULATION OF THE TOTAL DENSITY OF STATES

We shall denote by $P_n(M, I, G)$ the probability that a fireball of mass M , isospin I , and G parity G decays into n pions. The third component of isospin does not appear as a label since for $I < 2$ (we do not allow for exotic fireballs), it can be shown⁹

$$\begin{aligned} \tilde{P}_n(M, I, G) = & \sum_P (2S_2 + 1) \sum_{n_2} \kappa(n_2) \int_{m_{\min}}^{M-n_2 m_\pi} dm_1 \int_{n_2 m_\pi}^{M-m_1} dm_2 \rho(m_2) A(M, m_1, m_2) \delta_{G, G_1 G_2} \\ & \times \{ \delta_{I_1 0} [\delta_{I_2 0} \tilde{P}_{n-n_2}(m_1, 0, G_1) + \delta_{I_2 1} \tilde{P}_{n-n_2}(m_1, 1, G_1)] \\ & + \delta_{I_1 1} [\delta_{I_2 0} \tilde{P}_{n-n_2}(m_1, 1, G_1) \\ & + \delta_{I_2 1} (\tilde{P}_{n-n_2}(m_1, 0, G_1) + \tilde{P}_{n-n_2}(m_1, 1, G_1))] \} \\ & + \tilde{P}_{\text{initial}}(M, I, G), \end{aligned} \quad (10)$$

where we have summed over all possible light particles. Here, $\kappa(n_2)$ is the branching ratio of particle $P(m_2)$ into n_2 pions and $\rho(m_2)$ is its mass distribution. $A(M, m_1, m_2)$ is the two-body phase-space factor

$$\begin{aligned} A(M, m_1, m_2) = & \frac{V}{(2\pi)^3} \frac{\pi}{2M^4} [M^4 - (m_1^2 - m_2^2)^2] \\ & \times \lambda^{1/2}(M^2, m_1^2, m_2^2). \end{aligned} \quad (11)$$

The lower limit of integration m_{\min} is simply determined by the zeros of $\lambda^{1/2}(M^2, m_1^2, m_2^2)$.

that in a statistical model the decay is symmetric in isospin space. Following Margolis *et al.*,⁹ we now define an auxiliary probability:

$$\tilde{P}_n(M, I, G) = \rho(M, I, G) P_n(M, I, G), \quad (5)$$

where $\rho(M, I, G)$ is the isospin- and G -parity-dependent density of states. Clearly, the normalization condition reads

$$\sum_n P_n(M, I, G) = 1. \quad (6)$$

We thus have

$$\sum_n \tilde{P}_n(M, I, G) = \rho(M, I, G) \quad (7)$$

and the probability that a fireball decays into n pions is given by

$$P_n(M, I, G) = \frac{\tilde{P}_n(M, I, G)}{\sum_n \tilde{P}_n(M, I, G)}. \quad (8)$$

Consider, for instance, the process

$$F(M) \rightarrow F_1(m_1) + P(m_2) \rightarrow n\pi, \quad (9)$$

where $F_1(m_1)$ is a fireball of mass m_1 , of four-momentum q_1 , of isospin I_1 , and of G parity G_1 and $P(m_2)$ is a light particle of mass m_2 , of four-momentum q_2 , of isospin I_2 , of G parity G_2 , and of spin S_2 .

Generalizing the Frautschi bootstrap equation making use of the appropriate Clebsch-Gordan coefficients, we obtain with the above definition

We thus obtain a recursion relation independent of the density of states of any fireball which, given appropriate initial conditions, allows us to calculate explicitly the density of states for any M , I , and G .

Clearly, every resonance with compatible quantum numbers can be produced. Here, we shall allow for the emission of π , η , ρ , ω , η' , δ , f , A_2 , and g . All these resonances have a width of the order of the pion mass or less. Resonances such as ϵ , A_1 , ρ' , and A_3 are not so well established and shall be considered as kinematical effects.

For instance, broad structures in the A_1 and A_3 regions are predicted by the statistical bootstrap model as statistical enhancements.^{1,8,10}

We shall neither allow for the production of strange fireballs which, according to Zweig's rule are strongly suppressed—thus direct emission of kaons or of strange resonances will not be taken into account—nor for the emission of nonstrange resonances such as S^* , ϕ , and D which decay mainly into kaons. Empirically, we know that at high energy the amount of kaons is about ten times smaller than the amount of pions.¹¹ On the other hand, our model does not reflect this SU(3) symmetry breaking in the coupling constants and would overestimate the amount of kaons produced. Finally, due to their high masses, baryon production is negligible in the relatively low-mass range we shall be dealing with.

Therefore, the only vertices considered are those shown in Fig. 2. In these, photons have been counted as neutral pions. The mass distribution of very narrow resonances like π , η , ω , and η' have been taken to be Dirac δ functions, while the following relativistic Breit-Wigner distribution¹² has been used for the larger ones:

$$\rho(m) = \frac{2mm_0}{\pi} \frac{\Gamma(m)}{(m_0^2 - m^2)^2 + m_0^2 \Gamma^2(m)}. \quad (12)$$

$\Gamma(m)$ is given by

$$\Gamma(m) = \Gamma_0 \left(\frac{q}{q_0} \right)^{2l+1} \frac{2q_0^2}{(q^2 + q_0^2)}, \quad (13)$$

where

$$q = \frac{1}{2m} \lambda^{1/2}(m^2, m_1^2, m_2^2), \quad (14)$$

Γ_0 and l are, respectively, the width at $m=m_0$ and the spin of particle m_0 , while m_1 and m_2 are the masses of the decay products. This form had originally been chosen for the ρ resonance¹³ but we shall adopt it for any two-body resonance of spin l .

However, Dirac δ functions were taken for all resonances which start contributing to $\tilde{P}_n(M, I, G)$ at $n=6$ or higher. Their production rates are small and the use of a finite width would not change the result appreciably while complicating its evaluation.

Initial conditions that we used can be found in Ref. 5, one example of which is

$$\begin{aligned} \tilde{P}_3(M, 1, -) = & 0.38S(M, m_\eta, m_\pi) + 3S(M, m_\rho, m_\pi) \\ & + 0.02S(M, m_{\eta'}, m_\pi) \\ & + 4.05S(M, m_f(f-2\pi), m_\pi) \\ & + 1.68S(M, m_g(g-2\pi), m_\pi), \end{aligned} \quad (15)$$

where

$$\begin{aligned} S(M, m_1, m_2) = & \int_{m_3+m_4}^{M-(m_5+m_6)} dm_1' \rho(m_1') \\ & \times \int_{m_5+m_6}^{M-m_1'} dm_2' \rho(m_2') A(M, m_1', m_2'). \end{aligned} \quad (16)$$

Here, m_3 and m_4 are the masses of the decay products of particle 1 and m_5 and m_6 are those of particle 2.

Figure 3 shows the resulting density of states. A summation up to $n=15$ has been necessary to ensure a very good convergence over the whole range considered. We have used a volume of radius 1.1 fm, a value favored by Margolis *et al.* in e^+e^- annihilation⁹ and in other reactions.^{8,14} Above

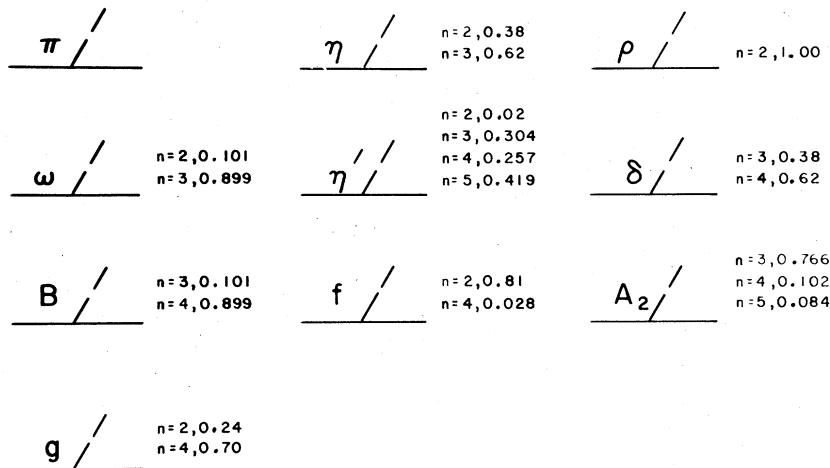


FIG. 2. Vertices taken into account in the linear bootstrap model to calculate the total density of states. Branching ratios into different number of pions are also given.

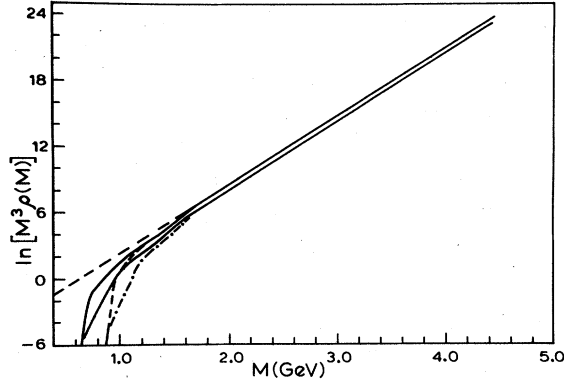


FIG. 3. $\ln [M^3 \rho(M, I, G)]$ vs M for different isospin and G -parity combinations. Upper full curve: $I^G=1^-$; lower full curve: $I^G=0^-$; short-dash curve: $I^G=1^+$; dash-dot curve: $I^G=0^+$; long-dash curve: continuation of the asymptotic form to low masses.

1.6 GeV, we observe a rather weak dependence on the quantum numbers of the fireball. Indeed, both $I=0$ and $I=1$ curves can clearly be parametrized with the same analytic function $\rho(M, I, G) = a_I e^{M/T} / M^3$ and the same parameters ($T=160$ MeV) except for overall normalization constants which are slightly different. We note a complete independence of the G parity for each isospin.

At lower mass, Eq. (10) does not really apply since the recursion relation does not account for discrete resonances, i.e., π , ρ , etc., which constitute the low-mass density of states. But there a direct counting of states¹⁵ leads to the same analytic form provided the denominator is replaced by $(M+M_0)^3$ to avoid the divergence at the origin. Thus we can use the asymptotic density of states over the entire range. It is clear, however, that a full statistical behavior is not expected to set in in the discrete resonance region and that results obtained there should be interpreted cautiously.

III. APPLICATION TO PION-PROTON SCATTERING

A. Contribution of two-particle vertices

We now proceed to evaluate the production cross section of n charged pions. Only a subset of all diagrams building up the total density of states contribute to such exclusive channels. In pion-proton scattering, the only vertices contributing are those shown in Fig. 4. But since the only particles produced are either charged pions or resonances decaying into charged pions, we no longer have isospin symmetry and cannot embody every case into a single recursion relation. However, interestingly, it turns out that we can write two different recursion relations, each being independent of the third component of isospin and actually of the G parity as well. The first holds for odd numbers of pions and the second for even numbers. These relations are

$$\begin{aligned} \tilde{P}_n(M, 1) = & \sum_P (2S_2+1)C(P) \sum_{n_2} \kappa(n_2) \int_{m_{\min}}^{M-n_2 m_\pi} dm_1 \int_{n_2 m_\pi}^{M-m_1} dm_2 \rho(m_2) A(M, m_1, m_2) \\ & \times \left\{ \left(\sum_{P_1=\pi, A_2} \delta_{PP_1} \right) [\tilde{P}_{n-n_2}(m_1, 0) + \frac{1}{2} \tilde{P}_{n-n_2}(m_1, 1)] \right. \\ & \left. + \left(\sum_{P_1=\rho, f, g} \delta_{PP_1} \right) \tilde{P}_{n-n_2}(m_1, 1) \right\} \\ & + \tilde{P}_{\text{init}}(M, 1) \quad (\text{if } n \text{ is odd}), \end{aligned} \quad (17)$$

where $C(P)$ ($=1$ for π, f ; $=\frac{1}{2}$ for A_2, ρ, g) are appropriate Clebsch-Gordan coefficients, and

$$\begin{aligned} \tilde{P}_n(M, 1) = & \sum_P (2S_2+1)C(P) \sum_{n_2} \kappa(n_2) \int_{m_{\min}}^{M-n_2 m_\pi} dm_1 \int_{n_2 m_\pi}^{M-m_1} dm_2 \rho(m_2) A(M, m_1, m_2) \\ & \times \left\{ \left(\sum_{P_1=\pi, A_2} \delta_{PP_1} \right) [\delta_{I_0 \frac{2}{3}} \tilde{P}_{n-n_2}(m_1, 1) + \delta_{I_1} \tilde{P}_{n-n_2}(m_1, 1)] \right. \\ & + \left(\sum_{P_1=\rho, f, g} \delta_{PP_1} \right) [\delta_{I_0 \frac{1}{3}} \tilde{P}_{n-n_2}(m_1, 1) + \delta_{I_1} \tilde{P}_{n-n_2}(m_1, 0)] \\ & \left. + \delta_{P_f} [\delta_{I_0} \tilde{P}_{n-n_2}(m_1, 0) + \delta_{I_1} \tilde{P}_{n-n_2}(m_1, 1)] \right\} \\ & + \tilde{P}_{\text{init}}(M, 1) \quad (\text{if } n \text{ is even}). \end{aligned} \quad (18)$$

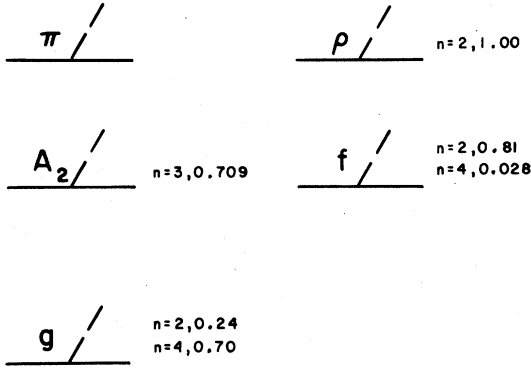


FIG. 4. Vertices contributing to the calculated exclusive channels in the linear bootstrap model. Branching ratios into different numbers of pions are also given.

Here, $C(P)=1$ for π , ρ , f , g and $\frac{1}{2}$ for A_2 . We note that for odd values of n , $\tilde{P}_n(M, 0)=0$. Initial conditions used to evaluate these recursion relations can be found in Ref. 5.

The fireball formation mechanism $R(s, t, M)$ is taken to be a triple-Pomeron exchange which dominates the cross section for small values of M^2/s .¹⁶ A PPR term could be added but would not affect our results appreciably.¹⁷

Figures 5–7 show our predictions for the five-, seven-, and nine¹⁸-pion mass spectra. We display three different contributions to stress the importance of adding all relevant contributions—in particular, resonance emission along or at the end of the chain—when generalizing the model to higher multiplicities. We note, however, that the simplest version of the model is sufficient to determine with good accuracy the mass of all enhancements.

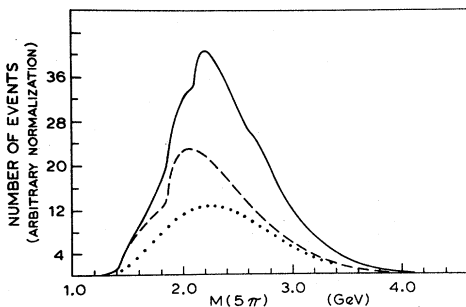


FIG. 5. Five-pion mass distribution in pion-proton scattering. The upper curve is the result of the full calculation; the middle curve takes into account only diagrams where the fireball decays into a pion plus another fireball—a pion plus a resonance at the end of the chain—[first term of Eqs. (17) and (18)]; the lower curve is the same as the middle one, but here all initial conditions yielding more than three pions have been removed.

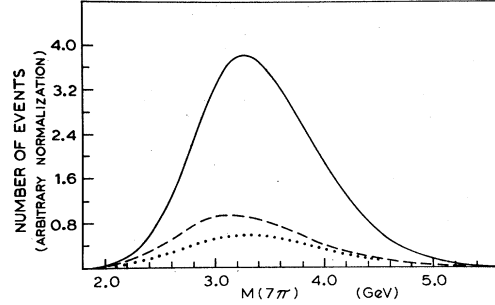


FIG. 6. Seven-pion mass distribution in pion-proton scattering. The curves are identified as in Fig. 5.

Three-pion enhancements are also predicted by the statistical bootstrap model as discussed in Refs. 1 and 8.

B. Contribution of three-pion vertices

So far, we have considered only a simpler version of the model in which a fireball decays into two particles. We shall now take into account the next dominant contribution: the decay of the fireball into three objects. Again here, we write recursion relations but since the diagrams are expected to contribute much less than the two-particle vertices, we neglect resonance widths. For the same reason, we shall not reevaluate the total density of states assuming *a priori* that the asymptotic temperature is not changed. From the results obtained, it will be easy to judge *a posteriori* if this was indeed a good guess.

Along the decay chain, the only vertices considered are those shown in Fig. 8. They are all of the type $\pi\pi F$ and πRF and dominate the nonlinear contribution. RRF vertices are suppressed because, firstly, the integrand is smaller for larger masses and, secondly, the integration interval is narrower. However, all $\pi\pi R$, πRR , and RRR vertices are allowed at the end of the chain.¹⁹ Thus, recursion relations in the nonlinear version of the model are

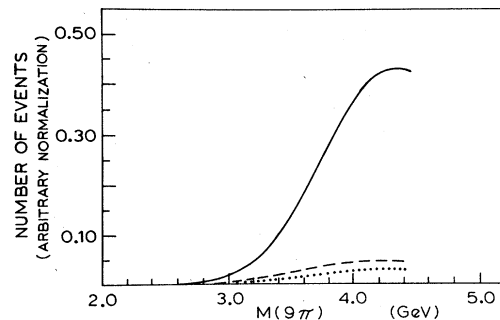


FIG. 7. Nine-pion mass distribution in pion-proton scattering. The curves are identified as in Fig. 5.

$$\begin{aligned}
\bar{P}_n(M, 1) = & \sum_P (2S_2 + 1)C(P) \sum_{n_2} \kappa(n_2) \int_{m_{\min}}^{M - (m_2 + m_\pi)} dm_1 I(M, m_1, m_2, m_\pi) \\
& \times \left\{ \left(\sum_{P_1=\pi, A_2} \delta_{PP_1} \right) \frac{2}{5} \bar{P}_{n-n_2}(m_1, 1) \right. \\
& + \left(\sum_{P_1=\rho, g} \delta_{PP_1} \right) \left[\frac{1}{2} \bar{P}_{n-n_2}(m_1, 0) + \frac{2}{5} \bar{P}_{n-n_2}(m_1, 1) \right] \\
& \left. + \delta_{Pf} \left[\bar{P}_{n-n_2}(m_1, 0) + \frac{1}{2} \bar{P}_{n-n_2}(m_1, 1) \right] \right\} \\
& + \text{terms of Eq. (17) (if } n \text{ is odd),}
\end{aligned} \tag{19}$$

$$\begin{aligned}
\bar{P}_n(M, I) = & \sum_P (2S_2 + 1)C(P) \sum_{n_2} \kappa(n_2) \int_{m_{\min}}^{M - (m_2 + m_\pi)} dm_1 I(M, m_1, m_2, m_\pi) \\
& \times \left\{ \left(\sum_{P_1=\pi, A_2} \delta_{PP_1} \right) \left\{ \delta_{I0} \left[\frac{2}{3} \bar{P}_{n-n_2}(m_1, 0) + \frac{1}{3} \bar{P}_{n-n_2}(m_1, 1) \right] \right. \right. \\
& \quad \left. \left. + \delta_{I1} \left[\bar{P}_{n-n_2}(m_1, 0) + \frac{4}{5} \bar{P}_{n-n_2}(m_1, 1) \right] \right\} \right. \\
& + \left(\sum_{P_1=\rho, g} \delta_{PP_1} \right) \left[\delta_{I0} \frac{1}{3} \bar{P}_{n-n_2}(m_1, 1) + \delta_{I1} \frac{4}{5} \bar{P}_{n-n_2}(m_1, 1) \right] \\
& \left. + \delta_{Pf} \left[\delta_{I0} \frac{2}{3} \bar{P}_{n-n_2}(m_1, 1) + \delta_{I1} \bar{P}_{n-n_2}(m_1, 1) \right] \right\} \\
& + \text{terms of Eq. (18) (if } n \text{ is even),}
\end{aligned} \tag{20}$$

where $C(P) = \frac{1}{2}$ for A_2 and 1 for π, ρ, f, g and where $n_2 = n_2 + 1$. Here $I(M, m_1, m_2, m_\pi)$ is the three-body non-invariant phase space⁵

$$I(M, m_1, m_2, m_3) = \frac{2\pi^2}{3} \frac{1}{n_i!} \int_{E_{2L}}^{E_{2U}} dE_2 \sqrt{X} \frac{E_2}{Y^3} \{3(M - E_2)^2 [Y^2 - (m_1^2 - m_3^2)^2] - X\}, \tag{21}$$

where

$$X = (E_2^2 - m_2^2)(Y - m_1^2 - m_3^2)^2 - 4m_1^2 m_3^2,$$

$$Y = M^2 - 2ME_2 + m_2^2,$$

$$E_{2L} = m_2,$$

$$E_{2U} = \frac{1}{2M} [M^2 + m_2^2 - (m_1 + m_3)^2],$$

and $1/n_i!$ is the statistical factor for n identical particles of type i .

Having done the calculation, we found firstly that the effect of these nonlinear diagrams on the shape of all spectra is totally negligible. Indeed, the new spectra, once properly renormalized, can be su-

perimposed within plotting accuracy on the old ones. Secondly, their effect on the magnitude of the cross sections is also pretty small and, as expected, slowly increases with the number of pions produced. This can be seen from Table I where the integrated branching ratios relative to the three-pion production cross section are given for all versions of the model presented here.

Therefore, it is clear that unless very precise experimental data become available the statistical bootstrap model, in its simpler linear version, is completely satisfactory. In addition, these results provide us with a full *a posteriori* justification for our use of an unmodified density of states. Three-particle vertices would contribute very

TABLE I. Multipion branching ratios in pion-proton scattering.

	Full calculation		Vertices: π/F	Vertices: π/F
	Linear	Nonlinear	Initial condition: π/R	Initial condition: π/ρ
			Linear	$\pi/f \rightarrow 2\pi, \pi/g \rightarrow 2\pi$
				Linear
$\sigma(3\pi)/\sigma(5\pi)$	7.57	7.46	12.99	19.83
$\sigma(3\pi)/\sigma(7\pi)$	60.9	59.0	234	353
$\sigma(3\pi)/\sigma(9\pi)$	~460	~447	~3533	~5957

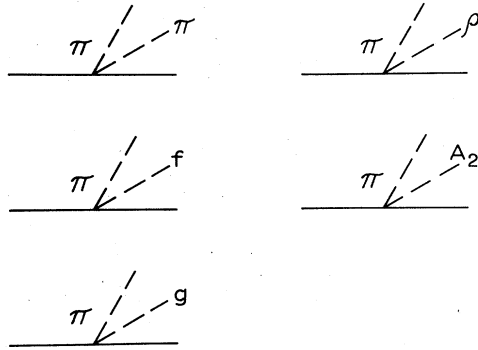


FIG. 8. Vertices taken into account to calculate exclusive channels in the nonlinear bootstrap model.

little, thus having a negligible effect on the temperature.

IV. APPLICATION TO PION-DEUTERON SCATTERING

It is an easy matter to extend the results obtained in Sec. III for pion-proton scattering to pion-deuteron scattering. Since in the latter case diffractive events are highly concentrated in the very-low- t region, multiple scattering is negligible. Thus, it is sufficient to multiply our results on hydrogen by the deuteron form factor and a relative normalization constant. We used²⁰

$$\frac{d\sigma_{\pi D}}{dM} = \left(\frac{\sigma_{\pi D}}{\sigma_{\pi P}}\right)^2 e^{-bt_{\min}} \frac{d\sigma_{\pi P}}{dM}, \quad (22)$$

where $t_{\min} = -[(M^2 - m^2)/2P_{\text{lab}}]^2$. Here m and M are the masses of the incident and outgoing particles, respectively, and b is a parameter related to the rms nuclear radius which can be extracted from experimental differential cross sections. It has been determined^{21,1,22} to be 30–32 GeV⁻² cor-

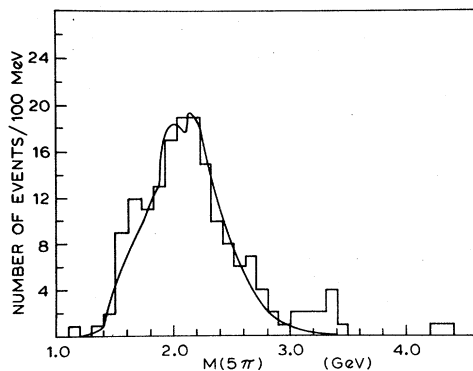


FIG. 9. Five-pion mass distribution in pion-deuteron scattering ($P_{\text{lab}} = 15$ GeV/c). Data from Ref. 1.

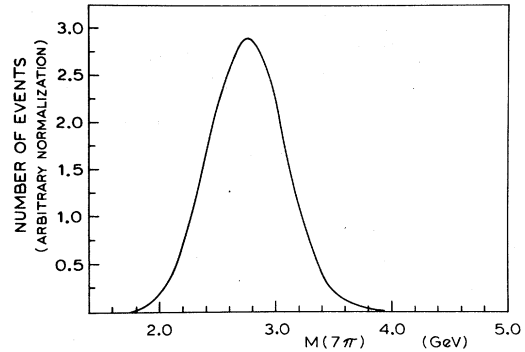


FIG. 10. Seven-pion mass distribution in pion-deuteron scattering ($P_{\text{lab}} = 15$ GeV/c).

responding to a radius of approximately 2.7 fm. However, we found our results insensitive to the precise value of b .

In the predicted spectra presented in Figs. 9–11, $b = 31$ GeV⁻² was selected. The agreement of the five-pion mass spectrum with data¹ is excellent; even structure details usually associated with dynamical effects are very satisfactorily explained. A prominent shoulder on the low-mass side is seen to be at least partly explained by our statistical picture, the result of competition among classes of diagrams peaking at somewhat different masses. The few unexplained events above 3 GeV may be due to some coherence setting up among the different partial waves and leading to Regge behavior.⁶

Integrated cross sections relative to the three-pion production cross section are displayed in Table II. It is obvious that the actual slope of the deuteron form factor is of little importance regarding the difficulty of measuring high-multiplicity events. Indeed, in this energy range ($P_{\text{lab}} = 15$ GeV/c), relative to the number of five-pion events,

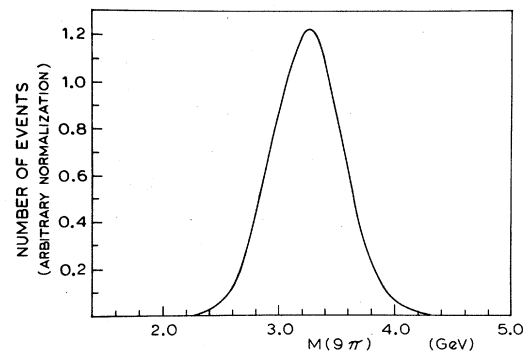


FIG. 11. Nine-pion mass distribution in pion-deuteron scattering ($P_{\text{lab}} = 15$ GeV/c).

TABLE II. Multipion branching ratios in pion-deuteron scattering at $P_{lab} = 15$ GeV/c. Normalization to hydrogen is provided by Eq. (22) with $(\sigma_{\pi D}^T/\sigma_{\pi p}^T)^2 = 3.6$. b is in GeV⁻².

	Full calculation				Vertices: π/F		Vertices: π/F	
	Linear		Nonlinear		Initial condition: π/R		Initial condition: π/ρ	
	$b = 31$	$b = 33.67$	$b = 31$	$b = 33.67$	Linear	Linear	$\pi/f \rightarrow 2\pi, \pi/g \rightarrow 2\pi$	Linear
$\sigma(3\pi)/\sigma(5\pi)$	17.19	18.12	16.94	17.87	26.71	27.97	46.38	48.87
$\sigma(3\pi)/\sigma(7\pi)$	1121	1320	1089	1284	3056	3532	5793	6716
$\sigma(3\pi)/\sigma(9\pi)$	2.82×10^5	3.87×10^5	2.70×10^5	3.78×10^5	1.10×10^6	1.45×10^6	2.11×10^6	2.79×10^6

only 1.6% yield seven pions. However, we have calculated that 21% of the absolute number of five-pion events obtained at $P_{lab} = 15$ GeV/c is reached in the seven-pion channel if $P_{lab} = 50$ GeV/c is used (28% at $P_{lab} = 100$ GeV/c).

The only available piece of data is the relative three-to-five-pion cross section. Lubatti and his collaborators¹ measured a ratio of 17.4 ± 3.5 in excellent agreement with our predictions for all versions of the full calculation. This is suggestive of some sort of precocious statistical behavior due to the rapid approach to the asymptotic density of states, certainly the best applicability criterion for our statistical model.

Finally, while the three-pion enhancement is basically easily identifiable two-body states ($\rho\pi, f\pi, g\pi$), we found the five-pion one to be the

sum of many diagrams of different numbers of steps in the decay cascade with no dominating single contribution. This is also in agreement with experiment.¹ In this regard, seven-pion measurements will be very interesting since, if this behavior persists, the statistical bootstrap model will provide a very reliable tool to predict the characteristics of high-multiplicity diffractive dissociation.

ACKNOWLEDGMENTS

It is a pleasure to thank Professor B. Margolis for useful suggestions and comments during the completion of this work. This work was supported in part by the Natural Sciences and Engineering Research Council of Canada and the Ministère de l'Éducation du Québec.

*Present address.

¹R. Harris *et al.*, Phys. Lett. **59B**, 187 (1975); Univ. of Washington Report No. VTL-PUP-43, 1977 (unpublished).

²F. Johns *et al.*, Phys. Rev. Lett. **29**, 756 (1972).

³R. Hagedorn, Nuovo Cimento Suppl. **3**, 147 (1965).

⁴S. C. Frautschi, Phys. Rev. D **3**, 2821 (1971).

⁵For a complete derivation of Eq. (1), see R. Gagnon, Ph.D. thesis McGill University, 1978 (unpublished). See also Ref. 6.

⁶B. Margolis, W. J. Meggs, and R. K. Logan, Phys. Rev. D **8**, 199 (1973).

⁷W. Nahm, Nucl. Phys. **B45**, 525 (1972).

⁸B. Margolis and S. Rudaz, Phys. Rev. D **9**, 653 (1974).

⁹B. Margolis, W. J. Meggs, and N. Weiss, Phys. Rev. D **13**, 2551 (1976).

¹⁰If the A_1 is a true resonance, its diffractive production will be accompanied by a large nonresonant background satisfactorily described by our model.

¹¹E. L. Feinberg, Phys. Rep. **5C**, 304 (1972).

¹²J. D. Jackson, Nuovo Cimento **34**, 1644 (1964).

¹³F. Selleri, Phys. Lett. **3**, 76 (1962).

¹⁴B. Margolis, W. J. Meggs, and S. Rudaz, Phys. Rev. D **8**, 3944 (1973).

¹⁵R. Hagedorn, Nuovo Cimento **52A**, 1336 (1967).

¹⁶Chan Hong-Mo *et al.*, Nucl. Phys. **B54**, 411 (1973); D. P. Roy and R. G. Roberts, *ibid.* **B77**, 240 (1974).

¹⁷The calculated spectra are indeed much more sensitive to the exponential dependence on M of the total density of states than to the polynomial dependence of the Pomeron-exchange term.

¹⁸The nine-pion mass spectrum was not calculated above 4.41 GeV. The integrated cross section was estimated by doubling the contribution up to this mass.

¹⁹Initial conditions used to evaluate Eqs. (19) and (20) can be found in Ref. 5.

²⁰U. Amaldi, M. Jacob, and G. Matthiae, Annu. Rev. Nucl. Sci. **26**, 385 (1976); F. Bradamante *et al.*, Phys. Lett. **31B**, 87 (1970).

²¹K. Paler *et al.*, Phys. Rev. Lett. **26**, 1675 (1971).

²²See Ref. 12 in Ref. 1.